CMTC-486020-MS

Static and Dynamic CO2 Storage Capacity Estimates of a Potential CO_2 Geological Sequestration Site in Louisiana Chemical Corridor

Muhammad Zulqarnain, Mehdi Zeidouni, Richard G Hughes, Louisiana State University

This paper was prepared for presentation at the Carbon Management Technology Conference held in Houston, Texas, USA, 17-20 July 2017.

Abstract

The close proximity of large CO_2 emitters and depleted oil and gas reservoirs in the Louisiana Chemical Corridor (LCC) provide unique opportunities for CO_2 geological sequestration in coastal Louisiana. The identification of sites with good storage capacity and retention characteristics is of prime importance for successful CO_2 storage projects. In this study, the Bayou Sorrel field area located within close proximity of some of the large CO_2 emitters in the LCC, is analyzed as a potential candidate site for aquifer storage. The results of static and dynamic aquifer storage capacity estimates are presented in this study. A volumetric approach is used to estimate the static storage capacity, and reservoir simulations are performed to compute dynamic storage capacity. The field and well data from publically available data sources are compiled to characterize the sands for prospective CO_2 sequestration intervals (i.e., non-productive sands), and pressure and temperature conditions.

Information of total areal extent, gross formation thickness, and total porosity are used along with a storage efficiency factor to find the pore volume available for storage. The upper depth limit for CO_2 injection is dictated by the pressure and temperature conditions at which CO_2 exists in a supercritical state. The Peng-Robinson (PR) equation of state is used in conjunction with subsurface pressure and temperature to determine the minimum depth at which CO_2 is supercritical. Multiple geological realizations are used for a realistic site specific storage capacity estimate. The reservoir simulations capture the transient nature of the process and provide estimation of storage capacity under dynamic conditions. The sensitivity of injection location and boundaries is also evaluated in the dynamic storage capacity estimates.

The results of the dynamic storage capacity estimate for a 1,000 ft thick interval at an average depth of 7,100 ft show that reasonable values of storage efficiency factors for this region are in the range of 1.14 to 2%. The results of the dynamic model also show that the nature of the storage zone boundary type, end point saturation and injection rate play significant role in estimation of dynamic storage capacity. These factors may induce more than 30% change in estimated dynamic storage value. The calculated storage efficiency factor may be applicable to other potential sites in this region, having similar geological characteristics.

Introduction

CO_2 can be stored in depleted oil and gas fields, deep saline aquifers or in coal seams or other formations that cannot be mined. Deep saline aquifers have the largest storage capacity amongst these. However, they also have the highest uncertainty in terms of their size and structural/stratigraphic traps as compared to hydrocarbon reservoirs (Jin et al., 2012) . CO_2 storage in saline aquifers is similar to CO_2 storage in depleted oil and gas reservoirs, the difference is in the water saturation (Bachu et al., 2007). Saline aquifers are initially saturated with water. This necessitates the estimation of site specific CO_2 storage values, a key component in selection of a storage site. The selected site must have enough pore volume available to meet the project economics, and at the same time it should retain the injected CO_2 for the lengthy duration necessitated by regulatory considerations. The economic considerations for a specific site may involve its close proximity to CO_2 sources, injection rates and pressure, number of wells required to achieve the desired injection rate, and combining storage with enhanced oil recovery (Goodman et al., 2011). The regulatory requirements includes protection of potable water sources, treatment of in-situ fluids, maximum injection limits to avoid any seismic event or fracture the rock, well spacing requirements and proximity to existing wells (Wilson, Johnson, & Keith, 2003). The Environmental Protection Agency (EPA)'s underground injection control (UIC) regulations incorporate most of these requirements (EPA, 2016). A potential sequestration site must meet both of the economics and regulatory requirements.

Capacity estimates

The site storage capacity estimates for CO_2 geological sequestration processes can broadly be categorized as static and dynamic. Volumetric and compressibility methods are two main static storage capacity calculation methods, while decline curve analysis, volumetric balance and reservoir simulation provide dynamic site specific CO_2 storage estimates. In this study volumetric and reservoir simulation are used as the static and the dynamic storage capacity methods respectively. A brief introduction of both of these methods follows.

Static storage capacity

The static estimates can be performed by using the petrophysical data of the proposed candidate site. In volumetric method the areal extent and height of target formation, formation pressure and temperature, porosity and storage efficiency factor are used. Initial pressure and temperature data is used to calculate the CO_2 density and then static storage efficiency is calculated by using the equation (1)

$$G_{CO_2 net} = A_t h_{net} \phi_{tot} \rho E_{net} \qquad (1)$$

where A_t= areal extent of sand, h_{net}= sand thickness, ρ is the CO_2 density at initial reservoir conditions, ϕ_{tot}= total porosity, and E_{net} is the storage efficiency factor. The storage efficiency factor reflects how much total pore volume is filled by CO_2. Its typical range is from 0.4 to 5.5 percent (Goodman et al., 2011). In saline aquifers it accounts for net to total area ratio that is suitable for CO_2 storage $E_{An/At}$, net to gross sand thickness $E_{hn/hg}$, and effective to total porosity$E_{\phi e/\phi tot}$. These terms account for the volume that is available to CO_2 sequestration. The areal E_A, microscopic E_d, vertical E_L and gravitational E_g sweep efficiencies take into account different barriers that prevent CO_2 from contacting 100% of the pore volume available. This is defined by the equation (2), (Goodman et al., 2011)

$$E_{saline} = E_{An/At} E_{hn/hg} E_{\phi e/\phi tot} E_A E_L E_g E_d \qquad (2)$$

The U.S. Department of Energy has specified some ranges of values for these terms (Goodman et al., 2011), which can be used to provide an initial guess for storage efficiency factor for a specific site.

Then dynamic storage capacity estimate described in next section can be used to verify the ranges for storage efficiency factor for that particular storage site.

Dynamic storage capacity

Numerical simulation, in principal, provides a realistic site specific storage capacity estimate, provided that a good data set for site characterization is available (Wallace, 2013) . The assumed value of storage efficiency factor can then be verified by using numerical simulations with an active injection scheme. In numerical simulations basic porous media fluid flow equations of continuity, momentum balance and energy balance are solved on grid cells. The simulations can address the relevant physical phenomenon of dissolution of CO_2 into brine, brine evaporation and salt precipitations (Ott, Roels, & de Kloe, 2015) and CO_2 mineralization over very long time durations.

The typical steps involved in reservoir simulations are the creation of a three dimensional geological model and estimation of petrophysical properties from available well log, core or past production data for the selected area. Then simulations are performed under various injection scenarios and sensitivity of the dynamic storage capacity to other uncertain parameters can studied. Dynamic capacity is highly influenced by the petrophysical properties of the storage zone. These petrophysical properties include porosity, permeability, and relative permeabilities and end point saturations of the phases. In addition, storage zone boundary types, initial pressure, initial temperature and injection rate influence the dynamic capacity estimates.

Injection rate is one of the critical elements in dynamic storage estimates. The injection rate is mainly decided by the project economics, formation fracture pressure and avoidance of creating any seismic events. Three high injection rates of 1, 1.5 and 2.64 MMt/y are used to study the impact of injection rate on dynamic storage capacity estimates.

In next sections we describe the steps involved in estimation of field specific static and dynamic CO_2 storage capacity estimates for deep saline aquifers.

Methodology

Bayou Sorrel is a nearly depleted oil/gas field and is located in Iberville Parish in Southern Louisiana with approximate location shown in Figure 1. Because the field has publically available data that extends from near surface through several aquifer zones into a deep productive interval, this data can be used to characterize the aquifer zones to show the process for both the static and dynamic estimation of storage volume.

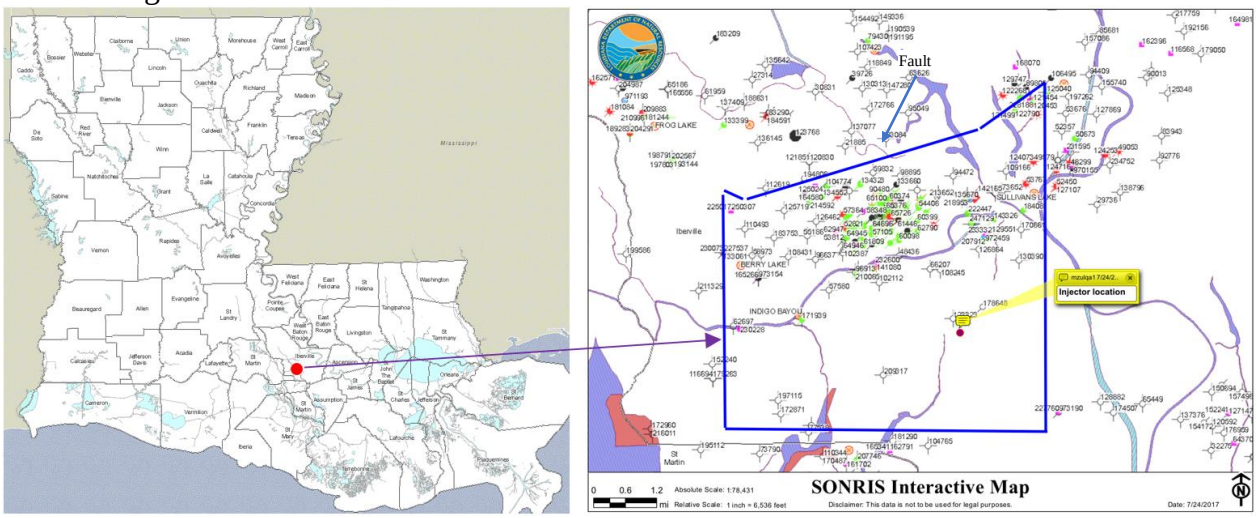

Figure 1: Approximate location and boundaries (shown by thick blue line) of potential candidate Bayou Sorrel site in southern Louisiana, U.S., approximate location of injector is also shown

The areal extent of the target region around the Bayou Sorrel field is approximately 26,000 acres. It is a stacked sand system. There are more than 21 sand intervals each of which has at least 80 ft thickness, spanning from 2,550 to 10,500 ft. A 1,000 ft thick zone at an average depth of 7,100 ft is selected for detailed static and dynamic capacity analysis. The results of the selected zones can be easily extrapolated to other zone if required to find the total storage capacity of this stacked sand system. The aquifer zones are similar to the productive interval in the field in that they are bounded by a fault along the northern edge of the area of interest. The fault has a throw of approximately 250 ft. The fault location is approximate as no seismic data was available. The injector location is selected to minimize wellbore leakage, by adopting the criteria specified in (Zulqarnain, Zeidouni, & Hughes, 2017). Therefore, it is located away from the main cluster of wells and is in a region where wells are sparsely located.

Site specific data

Site specific data was collected from the Louisiana Department of Natural Resources Strategic Online Natural Resources Information System (SONRIS). Well logs, production history, sand and well information can be obtained from this data source. The permeability data for this field is not available and therefore some uncertainty may be present in estimated permeability values.

Sand tops and net zone thickness

Raster well logs were all that was available in SONRIS. These raster logs were imported in the Petrel software system (Petrel, 2014), and sand tops were identified by cross sectional analysis. A total of 35 wells were used in delineating cross sections, running from west to east and north to south across the field. Some of the wells selected for cross section belong to neighboring fields or were dry holes, and were intentionally selected to examine the sand continuity to neighboring areas. A contour map of sand top for the zone of interest is shown in Figure 2 (a). It is an anticline structure cut by a fault of approximately 250 ft throw passing from the northeast to the southwest.

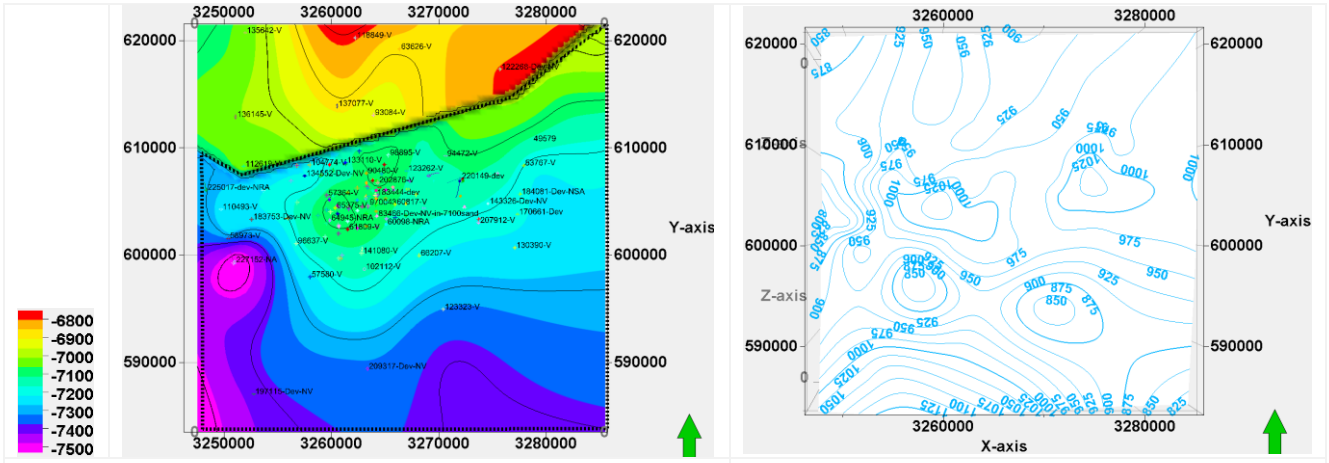

(a) Formation tops contour map (b) Sand thickness contour map

Figure 2: (a) Sand tops for the selected interval at an average depth of 7,100 ft depth, (b) average net thickness contour maps

The average total sand thickness is around 980 ft which is shown in the thickness map in Figure 2 (b). The sand does appear to be continuous in other neighboring areas as well.

Porosity and permeability

The facies and corresponding porosity value available from some of the well logs is reported in Table 1. The sand and shale intervals are identified by using a linear shale volume equation

$$V_{sh} = \frac{SP - SP_{CS}}{SP_{SH} - SP_{CS}}$$

where V_{sh} is the shale volume from SP curve, SP is the log value of SP curve, SP_{CS} average log value in the clean sand interval, SP_{SH} average log value in the pure shale. Four facies reported in Table 1 are defined for modeling purpose.

Table 1: Facies categorization and corresponding porosity range from well log data

Facies	Average Shale Content (%age)	Average Porosity %
Sand	0-10	29-33
Medium fine sand	10-30	24-29
Fine sand	30-80	18-24
Shale	80-100	12-18

This data was used to populate the 3D geological model used for static and dynamic storage capacity estimates. The effective porosity distribution in the injection area for an upscaled simulation model is shown in Figure 3. The average porosity in the interval is 28%, with a maximum porosity of around 33%. More than one geological realization for the porosity distribution was created and the results of only one of them are presented for brevity.

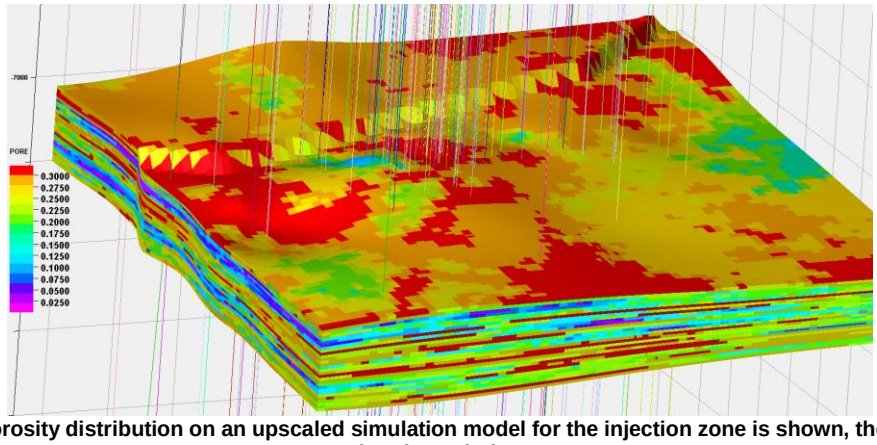

Figure 3: Effective porosity distribution on an upscaled simulation model for the injection zone is shown, the vertical line are well passing through the zone

Permeability and relative permeabilities

Both permeability and relative permeabilities play an important role in dynamic storage estimates. The core permeability data is not publically available for the selected site. An approximation of permeability is obtained by using Kozeny-Carman equation (Kozeny, 1927 and Carman, 1956) from the porosity distribution.

$$k = \frac{\phi^3 d^2}{72\tau(1-\phi)^2}$$

where ϕ is effective porosity, d is sand grain diameter and tortuosity τ is given by (Du Plessis & Masliyah, 1991)

$$\tau = \frac{\phi}{[1-(1-\phi)^{2/3}]}$$

In order to verify whether the estimated permeability values obtained from this equation are reasonable, initial production well test data available from well history files in (SONRIS) is used in a multiphase fluid flow simulator and the correlation was found to be reasonable. Then the results were extrapolated for the zone of interest to find the permeability in that zone. The resultant porosity-permeability plot is shown in Figure 4 (a). The relative permeability and end point saturations are also a critical element in determining the dynamic storage capacity (Burnside & Naylor, 2014). The relative

perm and capillary pressure data is extracted from (Krevor, Pini, Zuo, & Benson, 2012) and is representative of Berea sandstone. The relative permeability data is plotted in Figure 4 (b).

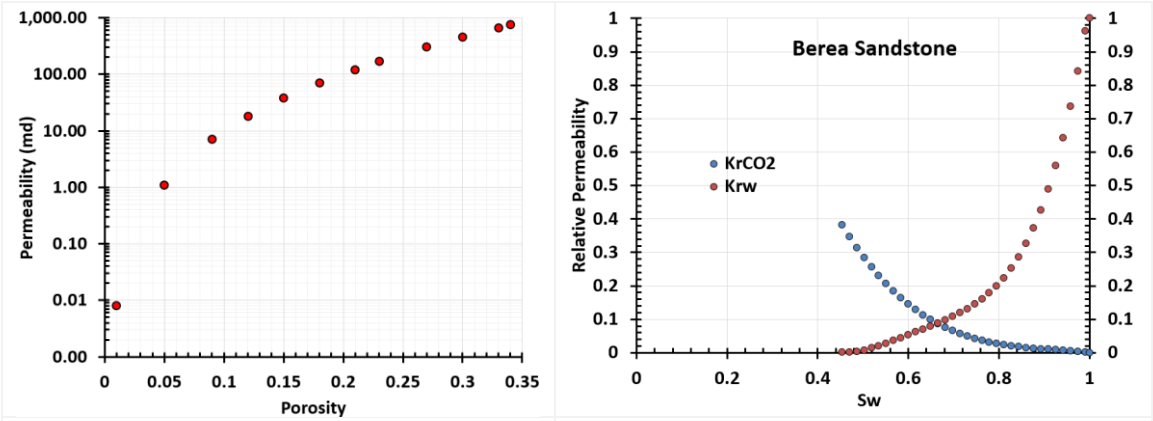

(a) Porosity permeability relationship (b) Fluid relative permeabilities

Figure 4: Permeability and relative permeability values for drainage

Pressure, temperature and CO_2 density

The geothermal gradient from the well log data is estimated to be 0.8ºF/100 ft. The formation pore, litho and fracture pressures calculated from the publically available data sources are shown in Figure 5. The formation is normally pressured with 0.465 psi/ft gradient (Nelson, 2012). Litho pressure is estimated from the sandstone formation with 2.65 g/cc density and average porosity of 28%. CO_2 density is calculated by using the Ping-Robinson equation of state (Peng & Robinson, 1976). All three parameter are shown in Figure 5.

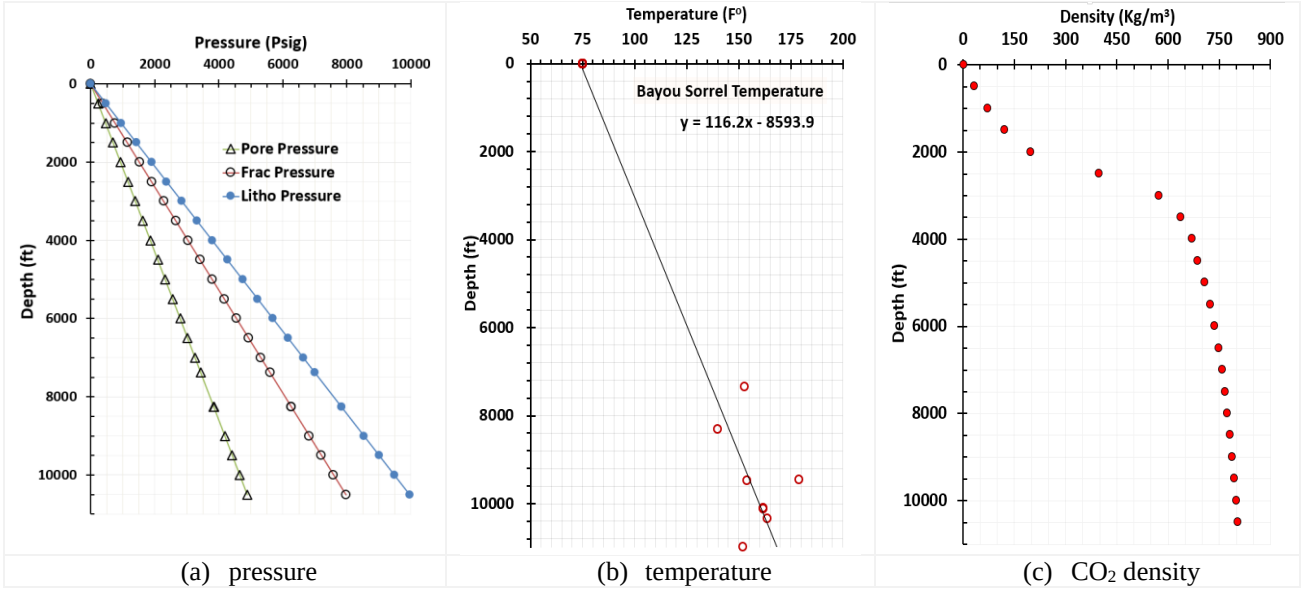

(a) pressure (b) temperature (c) CO_2 density

Figure 5: Pressure, temperature and density variations with depth for the selected site

Rock compressibility and water salinity

A uniform compressibility value was assumed. The formation compressibility is calculated by using the Hall's correlation

$$C_f = 1.87 \times 10^{-6} \phi^{-0.415}$$

where ϕ is the average porosity of the rock. Formation water salinity was estimated based on the apparent water resistivity and by using the log interpretation chart (Schlumberger, 2009). A value of

122,000 ppm was found corresponding to formation properties.

Results

Results for CO_2 static and dynamic capacity estimates are provided in this section.

Static storage capacity

Based on the available field data and considering the areal extent of the region, the results of the static storage capacity are provided in Table 2. With an average porosity of 28% and for a storage efficiency factor of 2%, the targeted sand can store up to 133 mega tons of injected CO_2 at reservoir conditions.

Table 2: Data used for preliminary static storage capacity estimates

Median Depth (ft)	Thickness (ft)	Area (ft^2)	Density (lb/ft^3)	Porosity Avg	Storage Efficiency factor	CO_2 Volume (MMt)
7300	980.00	1.13E+09	47.383	0.28	0.02	133.11

This is the storage capacity of one of the zones of interest. The Bayou Sorrel area has multiple zones at sufficient depth where CO_2 can exist in a supercritical state.

Dynamic storage capacity

The results of the dynamic storage estimate for one of the geological realization are presented in this section. Sensitivity of dynamic capacity to zone boundary type and injection rate is reported. CMG-GEM a commercially available reservoir simulation software that can model different chemical and mineral reactions of CO_2 during and after active period is used for numerical simulations (CMG-GEM, 2016). A grid with 79×79×30 blocks is used for numerical simulations. Grid block permeability values were assumed as isotropic in the horizontal directions, while vertical permeability is assumed to be 20% of the horizontal permeability. For a closed boundary the formation brine is not allowed to transmit across the zone boundaries, while for semi-closed and open system the brine is allowed to leave the storage zone. The semi-closed system is modeled by assuming a semi-infinite aquifer attached to the boundaries of the storage zone. For open boundaries an infinite acting aquifer is assumed.

Zone boundary sensitivity

The type of zone boundary plays an important role in estimation of dynamic capacity. Three scenarios for the storage zone boundary were considered: closed, semi closed and open boundaries. The simplistic and conservative approach is to consider that the targeted sand interval is a bounded system.

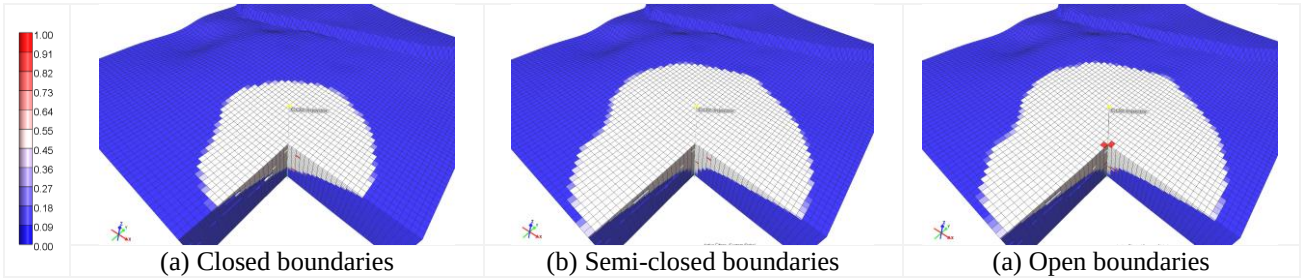

(a) Closed boundaries (b) Semi-closed boundaries (a) Open boundaries

Figure 6: CO_2 spatial saturation profile at the end of 50 year injection for (a) closed boundary, (b) semi closed, (c) and open boundary scenarios

For bounded system, no fluid or pressure transmission is allowed across boundaries. This essentially is the utilization of fluid and rock compressibility before the formation fracture pressure limit is reached. In this study 80% of the litho pressure is assumed as formation fracture pressure. The entire zone was perforated for CO_2 injection. The CO_2 saturation at the end of an injection period of 50 years is shown in Figure 6 for each of the storage zone boundary conditions.

Note that the CO_2 has the least spread in the case with a closed boundary condition, while for either semi-closed or open boundary conditions the spread is comparatively larger. The plume shapes and extent for semi-closed and open system are nearly identical. Note also that the well bottomhole pressure and injection rate plots, shown in Figure 7 are also required to completely understand the storage zone boundary effects.

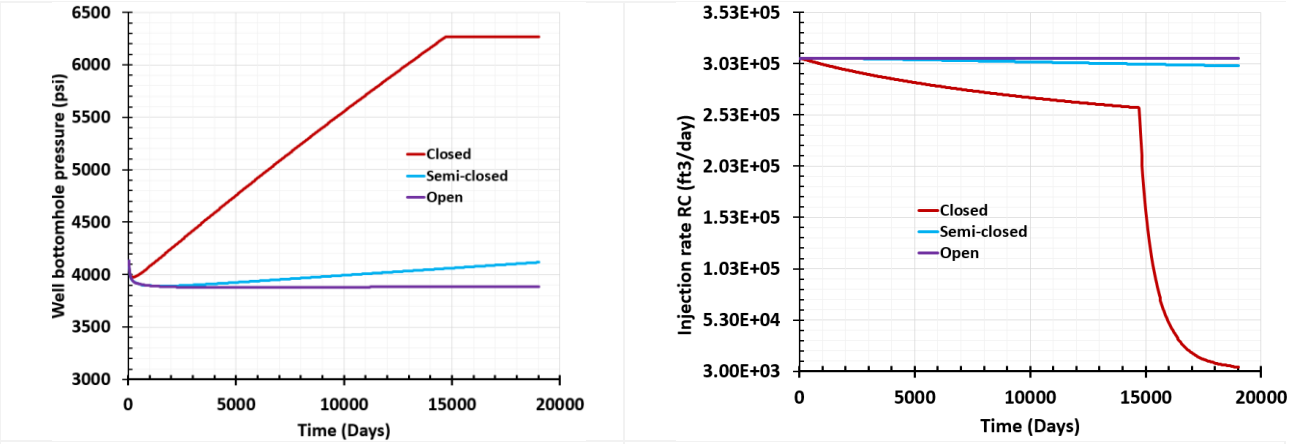

(a) well bottomhole pressure (b) injection rate

Figure 7: (a) Well bottomhole pressure and (b) injection rate for three boundary types

It can be observed from Figure 7(a), that for the closed boundary condition the well bottomhole pressure reaches its threshold value of 6247 psi. After that the injection rate shown in Figure 7 (b) significantly decreases to very low values. The pressure increase for either semi-closed or open boundary scenario is not significant, and therefore injection rates are not altered much. Therefore for closed boundary scenario, the injection is limited by the well's bottomhole pressure, while for the other two cases it is limited by the spread of the CO_2 plume. For semi-closed or open boundary type, the injection is stopped when the CO_2 front either reaches the delineated zone boundaries or the cluster of wells towards the northern boundary. The dynamic capacity estimate for the three boundary condition scenarios is shown in Table 3.

Table 3: Dynamic capacity estimate for three boundary types

Injection Rate (MMt/y)	Zone Boundary	Capacity (MMt)
2.46	Closed	93.50
	Semi-closed	129.59
	Open	132.22

It can be observed that the zone boundary is a significant factor in determining the dynamic capacity. An increase of nearly 40% is observed when the boundary type changes from closed to open.

Injection rate sensitivity

Injection rate is also another important parameter in estimation of dynamic storage capacity. For injection sensitivity analysis, an open zone boundary was assumed. The playoff between buoyancy and horizontal spread of CO_2 can be controlled by injection rate. The interplay between viscous and gravitational forces can be described by viscous to gravitational ratio (Withjack & Akervoll, 1988)

$$R_{v/g} = \frac{512 q \mu_d}{k \Delta \rho h^2}$$

where q is the injection rate (bbl/day), $\mu_d$is the brine viscosity (cp), k is permeability (md), $\Delta\rho$ is the density difference between brine and CO_2, h is the thickness of storage zone (ft). Higher this ratio is, better is the volumetric sweep efficiency. Therefore as we increase the injection rate, we get better sweep efficiency. For thick storage zones having lower injection rate the plume mostly moves into the upper portions of the zone alongside the caprock and most of lower portions of the zone remain untouched by CO_2, shown in Figure 8 (a).

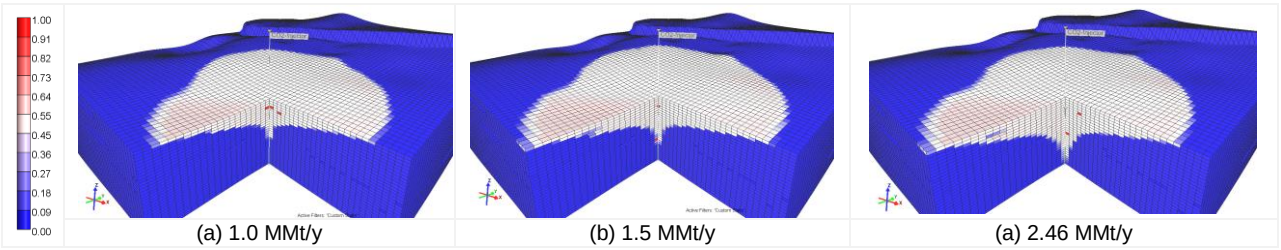

(a) 1.0 MMt/y (b) 1.5 MMt/y (a) 2.46 MMt/y

Figure 8: Plume spread for three injection rates, thickness is exaggerated to show the CO_2 sweep

As injection rate is increased from 1 to 2.46 MMt/y, the horizontal sweep efficiency of CO_2 increases, shown by the plume extent in Figure 8 (c). The results for the three injection rates are shown in Table 4.

Table 4: Dynamic storage capacity sensitivity to injection rate

Zone Boundary	Injection Rate (MMt/y)	$R_{v/g}$	Capacity (MMt)
Open	1	15.54	102.67
	1.5	23.264	109.41
	2.46	38.074	132.22

An increase of nearly 30% in dynamic storage capacity is observed when injection rate is increased from 1 to 2.46 MMt/y. Therefore optimization of the injection rate is also an important controlling parameter in dynamic storage estimates. It was also noticed in other cases, not reported here that for closed systems in which the plume extent is not a limiting factors, lower injection rate also yields good results. Therefore in order to select an injection scheme, it is critical to know the behavior of zone boundary types.

Summary and Conclusions

Static and dynamic saline aquifer CO_2 storage capacity estimates for a potential site in the Louisiana Chemical Corridor are performed. The volumetric method is used for the static capacity and numerical simulations are used for the dynamic capacity estimates. Publically available raster logs are used to build three dimensional geological models and in estimation of the petrophysical properties for these models. An average total porosity of 28% was estimated for a 1,000 ft thick zone of interest located at an average depth of 7,100 ft. Permeability data for the selected zone is estimated from correlations and is verified from initial production reports from producing wells in the oil and gas bearing zone. The estimated storage capacity ranges from 94 to 132 MMt, depending on the zone boundary type and operational conditions. This translates to storage efficiency factors in the range of 0.014 to 0.02. The selected example site is a stacked sand system with multiple thick sand zones having suitable conditions for supercritical CO_2 storage. Therefore the total storage capacity will be some multiple of the values reported in this study. This study highlights some of regional features and presents a suitable range of storage efficiency factors and therefore provides useful information for future regional studies and a process to follow to characterize the formations in those studies.

Nomenclature

E_{saline}	Saline aquifer storage efficiency factor
G_{CO_2net}	Net static storage capacity (MMt)
A_t	Total area of storage zone (m^2)
h_{net}	Net thickness of storage zone (m)
φ_{tot}	Total porosity
ρ	CO_2 density (Kg/m^3)
MMt	Million Mega tons
ϕ	Porosity
k	Permeability (mD)
τ	Tortuosity
d	Sand particle diameter (μm)
V_{sh}	Shale volume
C_f	Formation compressibility (1/psi)

Acknowledgement

The work is financially supported by U.S. Department of Energy for Carbon Storage Assurance and Facility Enterprise project (Grant # FE0029274).

References

Bachu, S., Bonijoly, D., Bradshaw, J., Burruss, R., Holloway, S., Christensen, N. P., & Mathiassen, O. M. (2007). CO2 Storage Capacity Estimation: Methodology and Gaps. *International Journal of Greenhouse Gas Control, 1*(4), 430-443. doi:http://dx.doi.org/10.1016/S1750-5836(07)00086-2

Burnside, N. M., & Naylor, M. (2014). Review and implications of relative permeability of CO2/brine systems and residual trapping of CO2. *International Journal of Greenhouse Gas Control, 23*, 1-11. doi:http://dx.doi.org/10.1016/j.ijggc.2014.01.013

CMG-GEM. (2016). Equation Of State (EOS) Compositional Simulator. Compuertr Modeling Group, Calgary, Canada.

Du Plessis, J. P., & Masliyah, J. H. (1991). Flow Through Isotropic Granular Porous Media. *Transport in Porous Media, 6*(3), 207-221. doi:10.1007/BF00208950

EPA. (2016). *Underground Injection Control Regulations and Safe Drinking Water Act Provisions*. Environmental Protection Agency, Title 40 of the Code of Federal Regulations, U.S. Government.

Goodman, A., Hakala, A., Bromhal, G., Deel, D., Rodosta, T., Frailey, S., . . . Guthrie, G. (2011). U.S. DOE methodology for the development of geologic storage potential for carbon dioxide at the national and regional scale. *International Journal of Greenhouse Gas Control, 5*(4), 952-965. doi:http://dx.doi.org/10.1016/j.ijggc.2011.03.010

Jin, M., Pickup, G., Mackay, E., Todd, A., Sohrabi, M., Monaghan, A., & Naylor, M. (2012). Static and Dynamic Estimates of CO2-Storage Capacity in Two Saline Formations in the UK. *SPE Journal*. doi:10.2118/131609-PA

Krevor, S. C. M., Pini, R., Zuo, L., & Benson, S. M. (2012). Relative permeability and trapping of CO2 and water in sandstone rocks at reservoir conditions. *Water Resources Research, 48*(2). doi:10.1029/2011WR010859

Nelson, P. H. (2012). Overpressure and Hydrocarbon Accumulations in Tertiary Strata, Gulf Coast of Louisiana. *Search and Discovery, August 2012*.

Ott, H., Roels, S. M., & de Kloe, K. (2015). Salt precipitation due to supercritical gas injection: I. Capillary-driven flow in unimodal sandstone. *International Journal of Greenhouse Gas Control, 43*, 247-255. doi:http://dx.doi.org/10.1016/j.ijggc.2015.01.005

Peng, D.-Y., & Robinson, D. B. (1976). A New Two-Constant Equation of State. *Industrial & Engineering Chemistry Fundamentals, 15*(1), 59-64. doi:10.1021/i160057a011

Petrel. (2014). Petrel: Exploration & Production Software Platform, Schlumberger Software Services, Houston, Texas USA.

Schlumberger. (2009). *Log Interpretation Charts*. Schlumberger Oilfield Services, Sugar Land, Texas, USA.

SONRIS. Strategic Online Natural Resources Information System, Louisiana Government, USA. Retrieved from http://www.sonris.com/

Wallace, K. J. (2013). *Use of 3-Dimensional Dynamic Modeling of CO 2 Injection for Comparison to Regional Static Capacity Assessments of Miocene Sandstone Reservoirs in the Texas State Waters, Gulf of Mexico.* (MSc), University of Texas at Austin Austin. Retrieved from https://repositories.lib.utexas.edu/handle/2152/21899

Wilson, E. J., Johnson, T. L., & Keith, D. W. (2003). Regulating the Ultimate Sink: Managing the Risks of Geologic CO2 Storage. *Environmental Science & Technology, 37*(16), 3476-3483. doi:10.1021/es021038+

Withjack, E. M., & Akervoll, I. (1988). *Computed Tomography Studies of 3-D Miscible Displacement Behavior in a Laboratory Five-Spot Model*. Paper presented at the SPE Annual Technical Conference and Exhibition, 2-5 October, Houston, Texas.

Zulqarnain, M., Zeidouni, M., & Hughes, R. G. (2017). *Risk Based Approach to Identify the Leakage Potential of Wells in Depleted Oil and Gas Fields for CO2 Geological Sequestration*. Paper presented at the Carbon Management Technology Conference, July 17-20, Houston, Texas.